**PMAS**
Proceedings of the Mongolian Academy of Sciences

Vol. 64 No 02(254) 2025
*DOI - https://doi.org/10.5564/pmas.v65i02.4390*

**ARTICLE**

# Optimal UAV Flight altitude for Multispectral monitoring of Wheat growth in Bayantsogt, Mongolia

**Mandukhai Turuu[1], Battuya Sanjaakhand[1] and Odgerel Bold[2*]**

[1]*School of Engineering and Technology, Mongolian University of Life Sciences, Ulaanbaatar, Mongolia*
[2]*Disaster Studies Center, Research Institute, University of Internal Affairs Ulaanbaatar, Mongolia*

*ARTICLE INFO: Received: 27 Feb, 2025; Accepted: 26 Jun, 2025.*

**Abstract:** This study evaluated the growth stages of wheat crops in the agricultural fields of Bayantsogt Soum, Tuv aimag-province, Mongolia, using unmanned aerial vehicles (UAVs) equipped with multispectral cameras. Aerial imagery was captured at four spatial resolutions - 1.59 cm, 3.63 cm, 5.44 cm, and 11.35 cm - corresponding to flight altitudes of 30 m, 80 m, 120 m, and 250 m, respectively. Six vegetation indices (NDVI, GNDVI, LCI, NDRE, NDWI, and OSAVI) were calculated to evaluate their relationships with wheat biometric parameters. The determinant coefficient ($R^2$) values for these indices were: LCI (0.81), OSAVI (0.79), NDRE (0.76), NDVI (0.76), NDWI (0.75), and GNDVI (0.73). Regarding spatial resolution, the corresponding $R^2$ values were 0.62 (1.59 ± 0.46 cm), 0.87 (3.63 ± 0.02 cm), 0.88 (5.44 ± 0.06 cm), and 0.68 (11.35 ± 0.04 cm) respectively. The findings indicate that the optimal flight altitude for estimating wheat growth characteristics was 120 m, providing a high correlation at a resolution of 5.44 ± 0.06 cm. By contrast, imagery captured from 250 m demonstrated relatively lower correlation. Overall, this study highlights the potential of UAV-based multispectral imaging for efficient crop monitoring and suggests an optimal operational altitude for precision agriculture applications.

**Keyword:** *Multispectral UAV imagery, wheat growth stages, vegetation indices, NDVI, spatial resolution, crop monitoring;*

## INTRODUCTION

The integration of digital technologies into agriculture has played a critical role in enhancing productivity, sustainability, and decision-making. Among these technologies, unmanned aerial vehicle (UAV)–based multispectral imaging has become a key tool in precision agriculture, enabling efficient crop monitoring, field management, and resource allocation. Globally, UAV technology has evolved rapidly, offering high-resolution imaging, real-time data acquisition, and cost-effective surveying capabilities, and it has become an indispensable component of agricultural innovation.

In Mongolia, the application of satellite imagery and digital analysis in agriculture began in the early 2000s. For example, in 2007, B. Bayartungalag conducted land use classification in Orkhon aimag using Landsat data, and in 2008, B. Batbileg analysed crop characteristics in Bornuur Soum.

**Corresponding author, email: odgerel.b@uia.gov.mn* https://orcid.org/0000-0003-2575-8662

At that time, the widespread adoption of such technologies was limited due to the lack of high-resolution spatial data and restricted access to remote sensing tools. Subsequent efforts, however, demonstrated increasing interest in digital technologies for agricultural purposes. In 2015, G. Nyamdorj developed an image processing method, using the OpenCV library and WDM camera systems, to distinguish weeds in fallow land. A regression model based on HSV color parameters enabled threshold-based weed identification through image analysis.

The Fourth Industrial Revolution has further accelerated the introduction of smart technologies in Mongolian agriculture. UAVs equipped with multispectral and thermal sensors are now applied to support field-level decision-making, including crop health assessment, yield estimation, and targeted spraying. According to global market analysis, the agricultural UAV market is projected to grow from USD 1.1 billion in 2022 to USD 7.19 billion by 2032, reflecting a strong shift toward digital farming solutions.

International studies have demonstrated the potential of UAV-based multispectral imaging in agriculture. For instance, Mazzia et al. (2020) developed a deep learning framework that refines satellite-derived vegetation indices using high-resolution UAV imagery, improving the accuracy of crop status assessments in vineyards. Hossen et al. (2021) combined UAV-based multispectral imaging with laser-induced breakdown spectroscopy (LIBS) to estimate total nitrogen content in soils, offering a rapid and non-invasive method for soil health evaluation. Panthakkan et al. (2025) compared UAV-based RGB and multispectral vegetation indices in palm tree cultivation, showing that cost-effective RGB imaging can provide comparable performance to multispectral methods in certain applications.

Despite these advances, the adoption of UAV-based multispectral imaging in Mongolian agriculture faces challenges, including the development of regulatory frameworks, technical capacity, and system integration. Nevertheless, the technology holds significant potential to support sustainable agricultural practices and optimize resource use. This study investigates the practical application of UAV-based multispectral imaging in Mongolian wheat production, focusing on the assessment of growth stages at varying spatial resolutions. The objective was to identify the optimal flight altitude and evaluate vegetation index performance to support precision agriculture in the region.

## Study Area

The study was conducted in the wheat-growing areas of Bayantsogt Soum, located in Tuv (Central) aimag of Mongolia, at coordinates 105°47′0″ E, and 48°30″ N (Figure 1). Bayantsogt lies at an elevation ranging from 1,200 to 1,500 meters above sea level and is geographically situated within the Khangai mountain range, specifically at the range's southeastern edge, characterised by steep and rugged terrain. Climatically, the region experiences cold and dry conditions, with long, harsh winters and short, cool summers. The annual heat supply ranges between 2,000 and 2,500°C. The mean temperature in January is approximately -25°C, while July averages around +25°C. Annual precipitation varies from 300 to 400 mm, and the average wind speed is between 4 and 6 m/s. The region is also characterised by notable meteorological extremes. Strong winds (≥15 m/s) occur for approximately 10–20 days every year. Snowstorms are recorded on 5–10 days annually, while dust storms occur on 10–30 days. The stable snow cover period generally extends from November 20 to December 20. Bayantsogt falls within Zone III of Mongolia's snow, wetness, and icing classification. Wet snow typically occurs for 1–5 days, lasting 2–3 hours per event. Glazed frost is observed for 1–5 days (lasting 6–14 hours), and icing events occur 1 to 2 days every year, usually lasting 1–3 hours. Seasonal snowmelt and bare ground conditions typically begin between March 1 and 10 [1]. Topographically, the landscape consists of a mix of open plains, rolling hills, and low mountainous terrain, making it suitable for both livestock husbandry and crop cultivation, particularly wheat farming.

Vol. 64 No 02(254) 2025
DOI - https://doi.org/10.5564/pmas.v65i02.4390

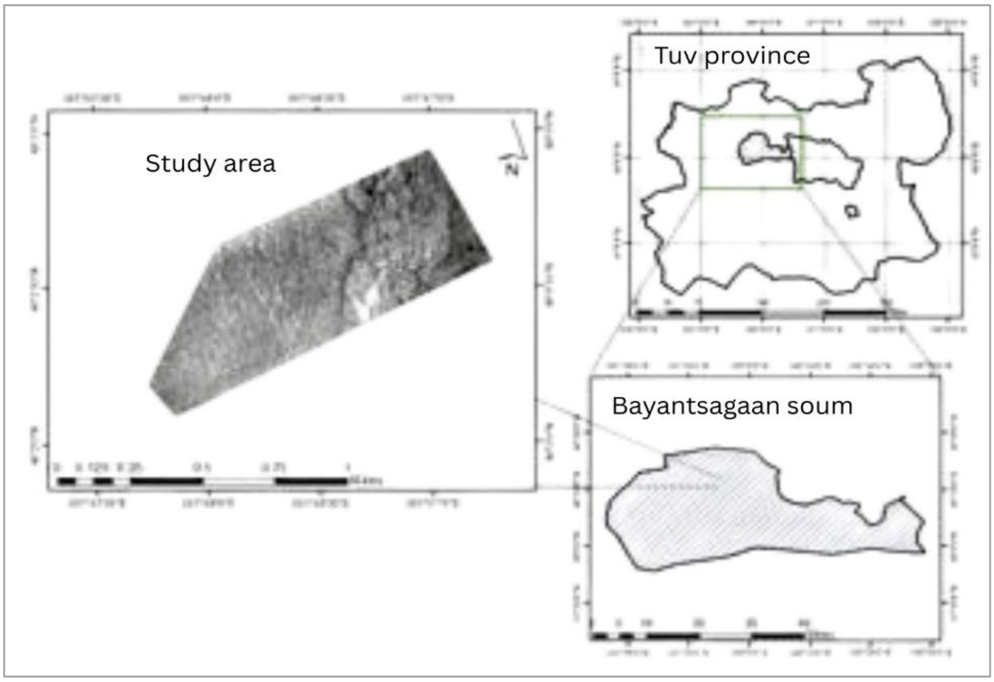


***Figure 1. Map of the study area. The field experiments were conducted in wheat cultivation areas of Bayantsogt soum, Tuv (Central) aimag, Mongolia, during the 2021 growing season.***

**Wheat Varieties**

In this study, the *Altaiskaya Yubileinaya* (*Triticum aestivum* L.) wheat variety was sown in the designated experimental field in Bayantsogt Soum during the first ten days of May 2021 [2]. This variety exhibits semi-erect plant architecture with a moderately dense, lanceolate to pyramidal spike structure, measuring approximately 6–8 cm in length. The spike lacks awns (beard), and the glumes are oval with obliquely narrow shoulders and slightly blunt, short teeth. The flowering scales are well-filled with grain. Leaves are of medium length and width, light green in color, and the flag leaf margins exhibit notable pigmentation. The flag leaf itself is semi-erect, and the plant has a medium-height stem. The grains are red, oval-shaped, with a slightly wrinkled surface, a deep and narrow groove, and a drooping base. The variety has a medium growth cycle, typically maturing in 82–89 days, that is, 2–3 days later than the *Altaiskaya 100* standard variety. According to varietal trials, its average yield was recorded at 21.4 t/ha. Under favorable conditions in the Altai region, yields reached 25.6 t/ha – exceeding the *Altaiskaya 100* variety by 3.5 t/ha. The highest recorded yield was 51.5 t/ha in Tyumen in 2013. Agronomically, *Altaiskaya Yubileinaya* is moderately resistant to drought and exhibits relative resistance to brown leaf rust. However, it is susceptible to diseases, such as Fusarium wilt, common bunt (*Tilletia* spp.), and septoria leaf blotch (*Septoria tritici*). Field observations indicate a low incidence of powdery mildew. The 1,000-kernel weight ranges from 32 to 39 grams. Grain quality metrics include a protein content of 13.5%, gluten content ranging from 22.7% to 29.6%, flour yield between 65.8% and 70.5%, it has a loaf volume of 360–375 $cm^3$, and an overall bread-making quality rating of 3.07 to 3.25. This variety has been cultivated in Mongolia since 2015 and was tested between 2015 and 2019 at the "Demonstration Field" of the Breeding Division, Mongolian University of Life Sciences (MULS). It performs particularly well in humid regions and demonstrates moderate drought tolerance [3].

**Data collection by UAV with Multispectral cameras**

In this study, a high-resolution multispectral imaging system was used for aerial data acquisition. The *MicaSense Altum* sensor (MicaSense Inc., Seattle, USA) (Figure 2b) was employed to capture both visible (Red, Green, Blue) and invisible (Red

Vol. 64 No 02(254) 2025
DOI - https://doi.org/10.5564/pmas.v65i02.4390

Edge, Near-Infrared) spectral bands, as well as thermal data. The spectral bands operate at the following central wavelengths and bandwidths: 668 ± 14 nm (Red), 560 ± 27 nm (Green), 475 ± 32 nm (Blue), 717 ± 12 nm (Red Edge), and 842 ± 57 nm (Near-Infrared) respectively. Each image was recorded in GeoTIFF format at a resolution of 2064×1544 pixels, with precise georeferencing. To ensure radiometric accuracy, the system was equipped with a calibrated reflectance panel (Figure 2c) and a Downwelling Light Sensor (DLS) (Figure 2d), which compensates for changes in ambient light during flights. For aerial platform deployment, the *DJI Matrice 210 RTK V2* UAV (Shenzhen, China) was selected due to its robust performance capabilities. The UAV features a 643 mm diagonal wheelbase, a maximum takeoff weight of 6.14 kg, and a top speed of 81 km/h. It supports wind resistance up to 12 m/s and operates efficiently at altitudes of up to 3000 m above sea level, with an operational temperature range from −20 °C to +50 °C (Figure 2a).

The maximum flight duration is approximately 33 minutes per charge. Environmental (e.g., dust, avian activity, irrigation systems) and meteorological conditions (e.g., cloud cover, wind, precipitation) significantly affect aerial image quality and subsequent data processing accuracy. To minimize these variables, aerial surveys were conducted under clear-sky conditions between 11:00 AM and 2:00 PM, during key phenological stages of wheat growth. The DJI Pilot software was used to execute autonomous flights at predetermined altitudes of 30 m, 80 m, 120 m, and 250 m respectively. Real-Time Kinematic (RTK) positioning was enabled via a mobile base station to improve spatial accuracy during data acquisition (Figure 2e).


***Figure 1. Unmanned aerial vehicle (a), Multispectral camera (b), Calibration plate (c), light sensor /DLS/ (d), Mobile GPS (e)***

**Field Sampling**

Phenological observations were conducted at four key growth stages of wheat - early growth, milk stage, heading (panicle) stage, and full maturity - by selecting five random sampling points within the wheat field. At each sampling point, a 50×50 cm quadrat frame was used for data collection.

Biometric measurements recorded included the number of plants, plant height, fresh biomass weight, leaf length, and leaf width. Specifically:

- *Plant density and tiller count per 1 m²:* Within the 50×50 cm quadrat, individual plants and tillers were counted and then extrapolated to a 1 m² area by multiplying by four.
- *Plant height (cm):* For each quadrat, the height of five randomly selected plants was measured from the base of the stem (soil surface) to the tip of the tallest leaf or stem, using a ruler. Measurements were taken at each growth stage.
- *Leaf length and width (cm):* Following Montgomery's (1911) approach for estimating leaf area from linear dimensions, the leaf length and maximum width of five randomly selected leaves within each quadrat were measured at all growth stages. Leaf area was calculated using the formula:
  Leaf Area=(Length×Width)×0.75\text{Leaf Area} = (\text{Length} \times \text{Width}) \times 0.75 Leaf Area=(Length×Width)×0.75.

PMAS
Proceedings of the Mongolian Academy of Sciences
Vol. 64 No 02(254) 2025
DOI - https://doi.org/10.5564/pmas.v65i02.4390

- *Seed count per 1 $m^2$:* At the uniform seeding stage, all seeds within the 50×50 cm quadrat were counted at five randomly selected points. The seed count was then multiplied by four to estimate the number of seeds per 1 $m^2$.
- *Yield estimation (t/ha):* The seed weight from the five quadrats (1 $m^2$ each) was measured, and yield was extrapolated to hectares, using the formula:

  T=A×10,000100=c (t/ha)T = \frac{A \times 10,000}{100} = c \text{ (t/ha)}T=100A×10,000=c (t/ha) where TTT is the estimated yield (t/ha), and AAA is the seed weight per 1 $m^2$ in kilograms.

- *Biomass measurement:* Aboveground biomass was harvested from all plants within the 50×50 cm quadrats at the five sampling points during July, August, and September of 2021. The fresh biomass was weighed, and net biomass weight was calculated by subtracting the weight of the collection bags:

  Net Biomass=Biomass with bag−Bag weight\text{Net Biomass} = \text{Biomass with bag} - \text{Bag weight}Net Biomass=Biomass with bag−Bag weight.

This systematic sampling approach ensured accurate characterisation of wheat growth and yield parameters across the developmental stages.

**Collection of Soil samples**

The soil types in Bayantsogt Soum of Tuv aimag span forest-steppe, steppe, and desert zones. Most agricultural fields in Bayantsogt are located within valleys surrounded by mountains and hills, featuring gentle slopes ranging from 0° to 3°. The dominant soil type in these agricultural lands is classified as light brown, typology of brown soil. Mechanically, the soil texture varies from light loam to sandy loam, making it suitable for the cultivation of a variety of crops. Regarding soil fertility, the thickness of the humus horizon within cultivated fields is variable, with the thinnest recorded depth at 20 cm and the thickest at 36 cm, averaging around 25 cm [4]. Soil sampling was conducted concurrently with wheat biometric measurements at five randomly selected points during different stages of plant growth: early tillering, milk stage, heading (panicle) stage, and full maturity. At each sampling point, four soil samples were collected from the 0–25 cm soil layer, with a combined minimum sample weight of 500 grams [8].

Sampling tools included shovels, measuring tapes, acrylic film bags for storage, and GPS devices for precise location recording. One soil profile was excavated per sampling site to represent the field's conditions. Agrochemical analysis of soils from the study area revealed that light loamy soils predominate, in terms of mechanical composition [21], [8]. The soil solution pH ranges between 7.8 and 8.0, indicating alkaline conditions, while soil salinity remains low, ranging from 0.04% to 0.06%. Nutrient analysis showed low humus content (1.52%–2.57%), sufficient levels of calcium and magnesium bases, very low nitrogen content (0.03–9.8 mg/kg), low phosphorus availability (0.5–1.5 mg/kg), and medium potassium levels (11–16 mg/kg).

## MATERIALS AND METHODS

### Spatial data analysis using UAV and Remote sensing

Multispectral aerial images were captured using a UAV equipped with a multispectral camera, flying at various altitudes. The collected data included multispectral images, geographic coordinates, flight altitude, and ambient light conditions.

These data were processed using *Pix4Dmapper* software [5], which applies advanced photogrammetry algorithms to integrate multiple overlapping aerial images. The processing workflow included radiometric and geometric corrections to ensure accuracy and consistency across datasets [6].

In total of 42,300 images acquired from 16 research flights were processed through three main stages:

Vol. 64 No 02(254) 2025
DOI - https://doi.org/10.5564/pmas.v65i02.4390

- Image integration - combining overlapping images to create continuous spatial coverage;
- Ground control point verification - ensuring spatial accuracy through reference points; and,
- Generation of thematic outputs - producing orthomosaics and other spatial products for further analysis.

This workflow produced high-quality orthomosaic images and additional spatial datasets necessary for subsequent vegetation index calculations and crop growth analysis.

*Table 1. Image resolution for each flight height, processing efficiency.*

| Flight height, m | Image resolution, cm/pixel | Image processing hour/min | Field size, ha |
|---|---|---|---|
| **30** | 1.59 ± 0.46 | 54.56 ± 11.03 | 3.31 ± 1.44 |
| **80** | 3.63 ± 0.02 | 26.28 ± 7.54 | 10.36 ± 1.74 |
| **120** | 5.44 ± 0.06 | 18.48 ± 3.48 | 18.27 ± 1.62 |
| **250** | 11.35 ± 0.04 | 58.28 ± 18.21 | 262.07 ± 29.48 |

Six vegetation indices were selected and analysed throughout the wheat growing season to assess plant health and development (see Table 2). *Image processing and spatial analysis* were performed using ArcGIS, a widely used platform for geographic information system (GIS) applications, regional mapping, and spatial projections. The input data for calculating these indices were multispectral images captured by the UAV's multi-channel sensors, including red (R), green (G), blue (B), near-infrared (NIR), and red-edge (RE) bands.

These vegetation indices provide key insights into various plant parameters, including chlorophyll content, biomass, and stress levels, enabling effective monitoring of crop growth and overall condition.

**Table 2. Plant spectral indices used in this study.**

| Name | Index | Index Calculation formula | Reference |
|---|---|---|---|
| NDVI | Normalised Difference Vegetation Index | (NIR − R) / (NIR + R) | Serrano 1998 |
| NDRE | Normalised Difference Red Edge Index | (NIR − RE) / (NIR + RE) | Barnes 2000 |
| NDWI | Normalised Difference Water Index | (Green − NIR) / (Green + NIR) | Pu 2008 |
| OSAVI | Optimized Soil-Adjusted Vegetation Index | (NIR − R) / (NIR + R + 0.16) | Rondeaux 1996 |
| GNDVI | Green Normalised Difference Vegetation Index | (NIR − Green) / (NIR + Green) | Fu-min 2007 |
| LCI | Leaf Chlorophyll Index | (NIR / RE) − 1 | Datt 1999 |

**Data Processing**

The relationships between variables were evaluated using Pearson's correlation coefficient (r), which quantifies the strength and direction of the linear association between two continuous variables. Values of r closer to ±1 indicate stronger correlations.

To examine the combined effects of multiple independent variables on a dependent

Vol. 64 No 02(254) 2025
DOI - https://doi.org/10.5564/pmas.v65i02.4390

variable, multiple regression analysis were conducted. The goodness of fit of the regression models was quantified using the coefficient of determination ($R^2$), representing the proportion of variance in the dependent variable explained by the independent variables (Equation 3).

The accuracy of spatial data predictions was further assessed using the Root Mean Square Error (RMSE), which measures the standard deviation of residuals (prediction errors) between observed and predicted values along the X and Y axes of the orthomosaic surface (Equation 4). RMSE provides an indicator of the average magnitude of errors in the model predictions, reflecting the overall precision of the spatial estimates.

$$R^2 = \frac{\Sigma_{i=1}^{n}(x_i-\bar{x})^2 \times (y_i-\bar{y})^2}{\Sigma_{i=1}^{n}(x_i-\bar{x})^2 \times \Sigma_{i=1}^{n}(y_i-\bar{y})^2} \quad (3)$$

$$RMSE = \sqrt{\frac{\Sigma_{i=1}^{n}(y_i-x_i)^2}{n}} \quad (4)$$

Correlation coefficients (*r*) and coefficients of determination (R2R^2R2) were calculated for each biometric phenological parameter of wheat, as well as for the corresponding vegetation indices, representing potential influencing factors.

## RESULTS AND DISCUSSION

### Multispectral UAV monitoring and Vegetation index analysis across Wheat growth stages

Measurement campaigns were conducted using a UAV, equipped with a multispectral camera, at four phenologically distinct growth stages of wheat: (1) heading, (2) milk ripeness, (3) dough ripeness, and (4) full ripeness. All flights were performed under consistent environmental conditions to ensure comparability, with each mission capturing high-resolution multispectral imagery across key spectral bands, including near-infrared (NIR), red edge (RE), red (R), and green (G).

Imagery was acquired at predetermined intervals corresponding to each growth stage, enabling temporal monitoring of crop development. From these images, vegetation indices, such as NDVI, GNDVI, and NDRE were derived to assess canopy structure, chlorophyll content, and physiological changes throughout the growth cycle (Figure 1, Table 2).

Analysis of the vegetation indices revealed stage-specific trends: for example, NDVI and NDRE values increased progressively from heading to dough ripeness, reflecting active biomass accumulation, whereas, slight decreases were observed at full ripeness, indicating maturation and senescence. GNDVI was particularly sensitive to chlorophyll variations, confirming its utility for monitoring nutrient status.

These findings demonstrate that UAV-based multispectral imaging provides a robust method for tracking wheat growth and detecting spatial heterogeneity within fields, supporting predictive modeling for yield estimation and stress detection. The observed trends align with previous studies: for instance, Mazzia et al. (2020) highlighted the enhancement of vegetation indices using high-resolution UAV imagery for crop status assessment, while Hossen et al. (2021) emphasised UAV-derived indices for rapid soil and plant health evaluation. Similarly, Panthakkan et al. (2025) demonstrated comparable performance between multispectral and RGB indices in assessing crop condition, indicating flexibility in sensor selection depending on operational constraints.

Overall, the results indicate that vegetation indices derived from multispectral UAV data are reliable indicators of wheat growth stages, and the approach can inform precise agriculture interventions, such as nutrient management, irrigation scheduling, and targeted pest control. However, optimal

Vol. 64 No 02(254) 2025
DOI - https://doi.org/10.5564/pmas.v65i02.4390

spatial resolution and flight altitude should be carefully considered to maximise correlation with biometric parameters, as confirmed by our analysis (Figure 2).

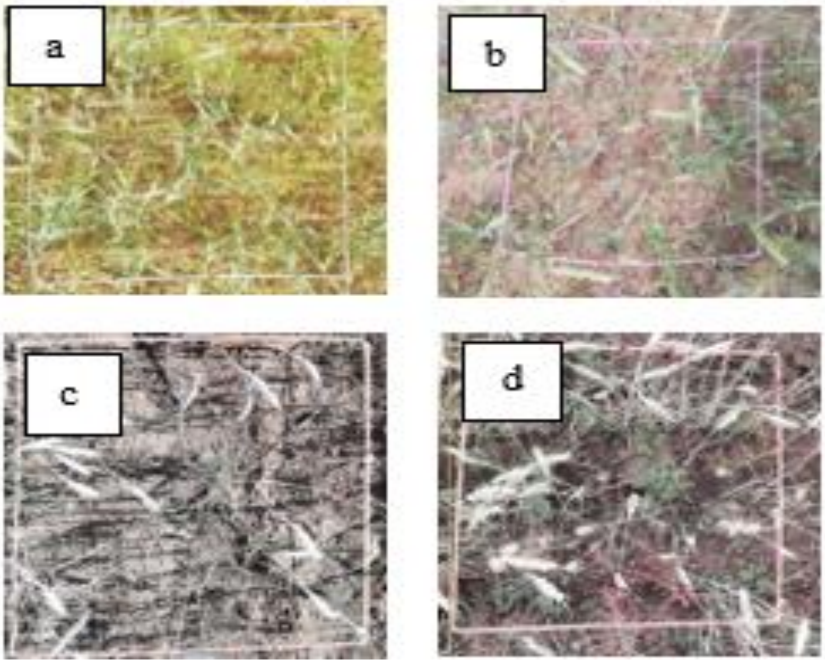


***Figure 3.*** *Visual representation of wheat development at four phenological growth stages as observed during UAV-based multispectral monitoring: a)* ***Heading stage*** *– the emergence of wheat spikes from the flag leaf sheath, indicating the onset of reproductive development; b)* ***Milk ripeness stage*** *– kernels are filled with milky fluid, representing active grain filling and high chlorophyll activity; c)* ***Dough ripeness stage*** *– kernels begin to firm as starch accumulation progresses, with leaves starting to senesce; d)* ***Full ripeness stage*** *– physiological maturity is reached, grain moisture content drops, and the canopy shows signs of desiccation.*

These stages were crucial for capturing variations in spectral reflectance, vegetation indices, and phenological transitions relevant for crop condition assessment and yield estimation.

**Analysis of Vegetation indices performance at Varying spatial resolutions**

Table 3 presents the root mean square error (RMSE) and coefficient of determination ($R^2$) for six vegetation indices - GNDVI, LCI, NDRE, NDVI, NDWI, and OSAVI - used to monitor wheat growth stages at four spatial resolutions: 30m, 80m, 120m, and 250m. These metrics provide insight into the accuracy and correlation strength between UAV-derived indices and ground-truth data across resolutions.

- GNDVI showed high performance at 120m resolution (RMSE = 0.03, $R^2$ = 0.85), indicating this resolution is optimal for capturing green biomass and chlorophyll variations. Its performance declined slightly at coarser (250m) and finer (30m) resolutions.
- LCI yielded the highest accuracy and correlation at 80m (RMSE = 0.02, $R^2$ = 0.92), making it highly effective for estimating leaf chlorophyll content and nitrogen status. Performance remained strong at 120m and 250m, but decreased at 30m.
- NDRE also performed best at 120m resolution (RMSE = 0.02, $R^2$ = 0.92), confirming its suitability for monitoring nitrogen-related changes and pigment levels. The trend of lower accuracy at 30m and 250m resolutions was consistent with other indices.
- NDVI showed a progressive improvement in $R^2$ values from 30m (0.65) to 120m (0.93), after which accuracy declined. This highlights that NDVI is sensitive to scale

Vol. 64 No 02(254) 2025
DOI - https://doi.org/10.5564/pmas.v65i02.4390

and performs optimally at intermediate resolutions.

- NDWI, useful for water content estimation, had its highest $R^2$ at 80m (0.85) but slightly lower performance at other resolutions, possibly due to noise from canopy moisture variability.
- OSAVI, which corrects soil background influence, showed robust performance at 120m ($R^2$ = 0.93), reinforcing the effectiveness of this resolution for mixed vegetation-soil environments.

***Table 3. Monitoring results based on vegetation indices during different wheat growth stages.***

| Index | 30m | | 80m | | 120m | | 250m | |
|---|---|---|---|---|---|---|---|---|
| | *RMSE* | $R^2$ | *RMSE* | $R^2$ | *RMSE* | $R^2$ | *RMSE* | $R^2$ |
| GNDVI | 0.17 | 0.61 | 0.04 | 0.81 | 0.03 | 0.85 | 0.07 | 0.65 |
| LCI | 0.08 | 0.59 | 0.02 | 0.92 | 0.03 | 0.91 | 0.12 | 0.83 |
| NDRE | 0.07 | 0.59 | 0.02 | 0.9 | 0.02 | 0.92 | 0.06 | 0.62 |
| NDVI | 0.15 | 0.65 | 0.06 | 0.87 | 0.05 | 0.93 | 0.13 | 0.59 |
| NDWI | 0.17 | 0.61 | 0.03 | 0.85 | 0.04 | 0.81 | 0.11 | 0.73 |
| OSAVI | 0.11 | 0.67 | 0.05 | 0.87 | 0.04 | 0.93 | 0.08 | 0.68 |

Overall, 80m and 120m spatial resolutions demonstrated superior accuracy and consistency across all vegetation indices. These findings suggest that intermediate spatial resolutions are optimal for UAV-based crop monitoring in wheat fields, balancing detail and coverage while minimising noise.

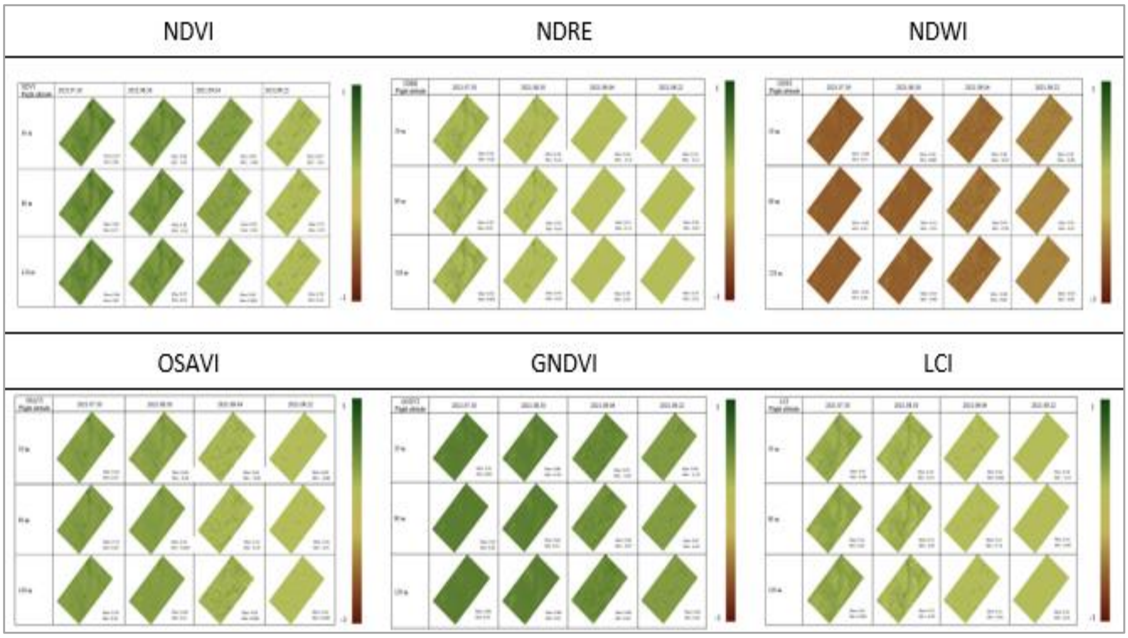


***Figure 4. Spatiotemporal distribution of vegetation indices (GNDVI, LCI, NDRE, NDVI, NDWI, OSAVI) captured by UAV flights at different altitudes (30m, 80m, 120m, 250m) across four wheat growth stages.***

PMAS
Proceedings of the Mongolian Academy of Sciences
Vol. 64 No 02(254) 2025
DOI - https://doi.org/10.5564/pmas.v65i02.4390

**Multispectral UAV Monitoring and Vegetation index analysis across Wheat growth stages**

Measurement campaigns were conducted using a multispectral camera-equipped UAV at four phenologically distinct wheat growth stages: (1) heading, (2) milk ripeness, (3) dough ripeness, and (4) full ripeness. Flights were carried out under consistent environmental conditions to ensure data comparability. High-resolution multispectral imagery was captured across key spectral bands, including near-infrared (NIR), red edge (RE), red (R), and green (G).

Vegetation indices - NDVI, GNDVI, NDRE, NDWI, OSAVI, and LCI - were derived from these images to assess canopy structure, chlorophyll content, water status, and physiological changes throughout the growth cycle (Figure 4). Temporal analysis revealed the following patterns:

- NDVI peaked at milk ripeness, reflecting high photosynthetic activity and dense green canopy, then declined during dough and full ripeness stages due to leaf senescence and reduction in biomass (Zhang et al., 2021; Li et al., 2020).
- NDRE, sensitive to chlorophyll and nitrogen content, gradually decreased after heading, indicating pigment degradation and reduced nitrogen availability (Mishra et al., 2019).
- NDWI peaked at milk ripeness, consistent with optimal plant water content, and decreased toward full ripeness, reflecting crop maturation and drying (Gao et al., 2021).
- OSAVI and GNDVI, which account for soil background effects and highlight leaf greenness, mirrored NDVI trends, peaking at milk ripeness and declining afterward (Rouse et al., 1974; Peñuelas et al., 1993).
- LCI sharply declined after dough ripeness, indicating chlorophyll reduction and lowered photosynthetic capacity (Hansen & Schjoerring, 2003).

Table 3 summarises the Root Mean Square Error (RMSE) and coefficient of determination ($R^2$) for each vegetation index at varying spatial resolutions (30 m, 80 m, 120 m, and 250 m). The analysis demonstrated that:

- NDVI, NDRE, and OSAVI performed optimally at 120 m flight altitude ($R^2$ = 0.92–0.93) supports intermediate-resolution imagery for accurate growth assessment.
- LCI achieved the highest accuracy at 80 m ($R^2$ = 0.92), particularly for monitoring chlorophyll and nitrogen status.
- GNDVI also showed strong performance at 120 m ($R^2$ = 0.85), highlighting its sensitivity to biomass and chlorophyll variations.
- NDWI peaked at 80 m ($R^2$ = 0.85), reflecting effective water content estimation, although slightly lower at other resolutions.

These findings indicate that UAV-based multispectral imaging provides a non-destructive, scalable method to monitor wheat growth stages, physiological status, and stress indicators. The study also suggests that intermediate flight altitudes (80–120 m) offer optimal spatial resolution for accurate vegetation index performance.

Figure 4. Temporal trends of six vegetation indices (NDVI, GNDVI, NDRE, NDWI, OSAVI, LCI) across wheat growth stages. Peaks indicate maximum photosynthetic activity, water content, and leaf chlorophyll levels, while declines correspond to senescence and maturation.

Table 3. RMSE and $R^2$ values for six vegetation indices at four UAV flight altitudes, demonstrating optimal performance at intermediate spatial resolutions.

Vol. 64 No 02(254) 2025
DOI - https://doi.org/10.5564/pmas.v65i02.4390

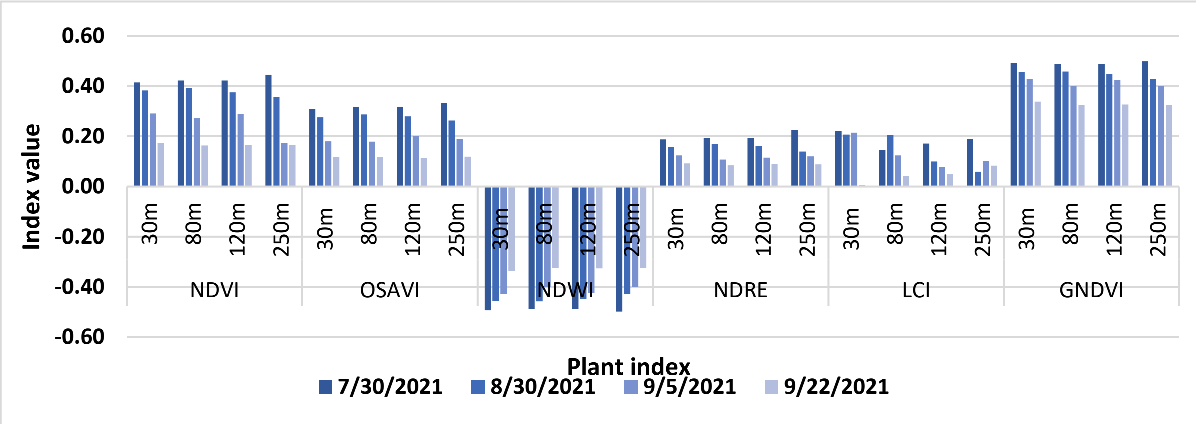


***Figure 5. Differences in Vegetation indices over time and Flight altitudes during the 2021 Wheat growin season.***

The figure illustrates the temporal dynamics of six different vegetation indices - NDVI, OSAVI, NDWI, NDRE, LCI, and GNDVI - across four distinct spatial resolutions (30 m, 80 m, 120 m, and 250 m) over a monitoring period from July 30 to September 22, 2021. The index values were derived from UAV-based multispectral data collected at four time points: July 30, August 30, September 5, and September 22 respectively. The x-axis represents each vegetation index subdivided by spatial resolution, while the y-axis shows the corresponding index values ranging from -0.6 to 0.6.

The bars are color-coded to indicate the observation dates, enabling visual comparison of temporal trends within and across indices and resolutions. Among the indices, the Normalised Difference Vegetation Index (NDVI) exhibited the highest values on July 30 across all spatial resolutions, indicating peak vegetation greenness during that period. A gradual decline in NDVI values over subsequent dates reflects the onset of vegetation senescence as the growing season progressed into autumn. A similar pattern was observed in the Optimised Soil-Adjusted Vegetation Index (OSAVI), which also declined steadily over time. OSAVI values tended to be slightly more stable at coarser spatial resolutions, likely due to the reduced influence of pixel-level variation and soil background effects. The Normalised Difference Water Index (NDWI), which estimates vegetation water content, showed consistently negative values (around -0.5) across all resolutions and time points. This indicates generally low moisture conditions within the crop canopy, which may be attributed to seasonal drying or drought-related stress. Notably, NDWI values further decreased over time, particularly from late August to mid-September.

The Normalised Difference Red Edge Index (NDRE), which is sensitive to chlorophyll content and plant physiological status, was highest at 30 m resolution in late July and declined markedly in later observations. Index values were lower at 250 m resolution, suggesting diminished sensitivity to subtle physiological changes at coarser scales. The Leaf Chlorophyll Index (LCI) also followed a declining trend, with relatively higher values observed at 30 m and 80 m resolutions in July. The reduction in LCI values toward September likely indicates a decrease in leaf chlorophyll concentration due to crop maturation and senescence. Finally, the Green NDVI (GNDVI), which is based on green light reflectance and similarly captures vegetation vigor, mirrored the trend seen in NDVI. Peak GNDVI values (~0.45) were recorded in July, followed by a steady decline across all spatial resolutions. The consistency of this pattern underscores the robustness of GNDVI as a proxy for vegetation health. In summary, all vegetation indices peaked in late July, coinciding with the crop's vegetative maximum, and declined thereafter as the wheat matured and approached the end of its life cycle.

Vol. 64 No 02(254) 2025
DOI - https://doi.org/10.5564/pmas.v65i02.4390

While some variation in index magnitude was observed across spatial resolutions, the overall temporal trends were consistent. The negative NDWI values and declining chlorophyll-sensitive indices (NDRE, LCI) provide further evidence of decreasing plant water content and photosynthetic activity during the latter stages of the growing season. These findings highlight the utility of multispectral UAV imagery for monitoring crop dynamics with both spatial and temporal precision.

Recent studies have underscored the critical role of spatial resolution in UAV-based remote sensing for accurately estimating wheat growth parameters such as biomass, leaf area index (LAI), and chlorophyll content. While your research identified a spatial resolution of 5.41 cm as optimal for correlating vegetation indices with wheat biometric indicators, other studies have explored a range of resolutions to determine their efficacy in various agronomic assessments. A study by Guo et al. [66] investigated the impact of UAV imagery at different spatial resolutions on SPAD (Soil Plant Analysis Development) values, which are indicative of chlorophyll content. They found that imagery with a spatial resolution of 1.8 cm/pixel, obtained at a flight altitude of 50 meters, provided the most accurate SPAD estimations. This suggests that higher spatial resolutions can enhance the precision of chlorophyll-related measurements. BioMed Central Yue et al. [18] demonstrated that integrating ultrahigh-resolution image textures with vegetation indices significantly improves the estimation of above-ground biomass (AGB) in winter wheat. Their research indicated that combining image textures from 1- to 30-cm ground-resolution images with vegetation indices yielded an $R^2$ of 0.89 and a root mean square error (RMSE) of 0.82 t/ha, outperforming models using only vegetation indices or image textures. Tao et al. utilised UAV-based hyperspectral images to estimate the yield and plant height of winter wheat. Their findings revealed a strong correlation ($R^2$ = 0.97) between UAV-extracted plant height and ground-measured plant height. Moreover, combining spectral indices with UAV-derived plant height data improved yield prediction accuracy, achieving an $R^2$ of 0.77 and an RMSE of 648.90 kg/ha.

These studies collectively highlight that while ultrahigh spatial resolutions (e.g., 1.8 cm/pixel) can enhance the accuracy of specific measurements, like chlorophyll content and biomass estimation, resolutions around 5 cm/pixel may offer a balance between data quality and operational efficiency for broader agricultural monitoring purposes. The integration of vegetation indices with additional data types, such as image textures and structural information, further refines the assessment of crop health and yield potential. In conclusion, selecting an appropriate spatial resolution for UAV-based monitoring should consider the specific agronomic parameters of interest, the desired accuracy, and the practical aspects of data acquisition and processing. Our finding of 5.41 cm as an optimal resolution aligns with the broader consensus that moderate spatial resolutions can effectively support comprehensive crop monitoring while maintaining operational feasibility.

## CONCLUSIONS

- The application of multi-spectral unmanned aerial vehicles (UAVs) enables high-precision spatio-temporal monitoring of wheat crop development, thereby providing reliable data to support informed decision-making in precision agriculture. The current study demonstrates the effectiveness of different vegetation indices (VIs) at multiple spatial resolutions in estimating key biometric parameters of wheat during distinct phenological stages.
- During the heading stage, the strongest correlations for estimating biomass wet weight were observed with NDVI (30 m, $R^2$ = 0.99), OSAVI (30 m, $R^2$ = 0.96), and LCI (30 m, $R^2$ = 0.85). For leaf length, NDRE (80 m, $R^2$ = 0.86) and NDVI (120 m, $R^2$ = 0.85) yielded the best results, while leaf width was best estimated by OSAVI (120 m, $R^2$ = 0.75). NDWI showed consistent negative correlations, suggesting its limited utility for structural parameters. UAV flights conducted at 1.59

cm and 5.44 cm spatial resolutions were optimal during this stage, whereas lower resolution (11.35 cm) flights showed weaker correlations. In the milk stage, biomass wet weight correlated most strongly with OSAVI (120 m, $R^2 = 0.96$), NDRE (120 m, $R^2 = 0.91$), and LCI (120 m, $R^2 = 0.93$). For leaf length, NDRE (120 m, $R^2 = 0.89$) and LCI (120 m, $R^2 = 0.81$) performed best. Plant height estimation was highly correlated with OSAVI (250 m, $R^2 = 0.95$), NDRE (120 m, $R^2 = 0.88$), and NDVI (250 m, $R^2 = 0.91$). Again, 5.44 cm spatial resolution emerged as optimal. During the dough stage, correlations weakened slightly. Biomass wet weight correlated best with OSAVI (120 m, $R^2 = 0.76$) and GNDVI (120 m, $R^2 = 0.70$). Leaf length showed moderate correlation with NDVI (250 m, $R^2 = 0.84$), while plant height was best estimated by GNDVI at 30 m and 120 m ($R^2 = 0.59$ and $0.55$, respectively). UAV imagery at 5.44 cm resolution remained most effective. In the full ripening stage, estimation of biomass wet weight was most successful with GNDVI (80 m, $R^2 = 0.71$), while plant height and plant count correlated best with NDWI (120 m, $R^2 = 0.64$) and LCI (250 m, $R^2 = 0.85$), respectively. Optimal flight altitudes for this stage were associated with spatial resolutions of 3.63 cm, 5.44 cm, and 11.35 cm, depending on the parameter assessed.

- When analysing overall correlation between spectral indices and wheat biometric characteristics, the highest average $R^2$ values were obtained with LCI ($R^2 = 0.81$), OSAVI ($R^2 = 0.79$), NDRE ($R^2 = 0.76$), NDVI ($R^2 = 0.76$), GNDVI ($R^2 = 0.73$), and NDWI ($R^2 = 0.75$). This confirms the utility of a range of vegetation indices, with LCI and OSAVI performing consistently well across phenological stages.
- The analysis also revealed that spatial resolution significantly influences correlation accuracy. At a high resolution of 1.59 ± 0.46 cm (30 m flight), the average $R^2$ was 0.62. This improved markedly at 3.63 ± 0.02 cm (80 m, $R^2 = 0.87$) and 5.44 ± 0.06 cm (120 m, $R^2 = 0.88$). However, at a coarser resolution of 11.35 ± 0.04 cm (250 m), correlation strength declined ($R^2 = 0.68$). These findings align with previous research suggesting that moderate to high spatial resolution (3–6 cm) provides a practical balance between accuracy and data processing efficiency for UAV-based crop monitoring.

## Acknowledgements

This research was conducted within the framework of the project funded by the United States Department of Agriculture (USDA) through Foreign Agricultural Service (FAS), under the grant number FX20SR-10961R006. The authors would like to express their sincere gratitude to Professor P. Stephen Baenziger of the University of Nebraska for his leadership and valuable guidance throughout the implementation of the project.

## Ethical Approval

This study did not involve any human or animal subjects and thus, did not require ethical approval. All research activities were conducted in accordance with institutional and national guidelines.

## Author Contributions

M.T. UAV data collection, vegetation index calculation, data analysis, manuscript drafting. B.S. Field observation, soil sampling, soil analysis, data organisation. O.B. Conceptualisation, methodology development, manuscript review, editing, and supervision. All authors have read and approved the final version of the manuscript**.**

## Source of Funding

This work was supported by the United States Department of Agriculture (USDA), Foreign Agricultural Service (FAS), under grant number FX20SR-10961R006.

## Conflict of Interest

The authors declare that they have no known competing financial interests or personal relationships that could have appeared to influence the work reported in this paper.

## REFERENCES


1. Barnes, E. M., Clarke, T. R., Richards, S. E., Colaizzi, P. D., Haberland, J., Kostrzewski, M., … Moran, M. S. (2000, July 16–19). *Coincident detection of crop water stress, nitrogen status, and canopy density using ground-based multispectral data*. In Proceedings of the 5th International Conference on Precision Agriculture (pp. 1–15). Bloomington, MN. https://www.indexdatabase.de/db/r-single.php?id=642&utm_source.
2. Banaszek, A., Zarnowski, A., Cellmer, A., & Banaszek, S. (2017). *Application of new technology data acquisition using aerial (UAV) digital images for the needs of urban revitalization*. In *Environmental Engineering: Proceedings of the 10th International Conference on Environmental Engineering (ICEE)* (Vol. 10, pp. 1–7). Vilnius Gediminas Technical University. https://doi.org/10.3846/enviro.2017.159.
3. Cauchard, J. R., Zhai, K. Y., Spadafora, M., & Landay, J. A. (2016). Emotion encoding in human-UAV interaction. In *2016 11th ACM/IEEE International Conference on Human-Robot Interaction (HRI)*. https://doi.org/10.1109/hri.2016.7451761.
4. Clevers, J. G. P. W., Kooistra, L., & van der Brande, M. M. M. (2017). Using Sentinel-2 data for retrieving LAI and leaf and canopy chlorophyll content of a potato crop. *Remote Sensing, 9*(4), p. 405. https://doi.org/10.3390/rs9040405.
5. Datt, B. (1999). Remote sensing of water content in eucalyptus leaves: The Leaf Chlorophyll Index (LCI). *Journal of Plant Physiology, 154*(1), pp. 30–36. https://doi.org/10.1016/S0176-1617(99)80125-6.
6. Giones, F., & Brem, A. (2017). From toys to tools: The co-evolution of technological and entrepreneurial developments in the UAV industry. *Business Horizons*, 60(6), pp. 875–884. https://doi.org/10.1016/j.bushor.2017.08.001
7. Gao, F., Zhang, L., & Wang, X. (2021). Water content estimation using UAV remote sensing. Agricultural Water Management, p. 247, 106694. https://doi.org/10.1016/j.agwat.2020.106694.
8. Honkavaara, E., & Khoramshahi, E. (2018). Radiometric correction of close-range spectral image blocks captured using an unmanned aerial vehicle with a radiometric block adjustment. *Remote Sensing*, 10(2), p. 256. https://doi.org/10.3390/rs10020256.
9. Hansen, P. M., & Schjoerring, J. K. (2003). Leaf chlorophyll measurement using spectral indices. Photosynthetica, 41(3), pp. 303–305. https://doi.org/10.1023/A:1023960623095.
10. Hossen, M. I., Al-Tamimi, A., Salah, M., & Al-Habaibeh, A. (2021). Soil nitrogen estimation using UAV-based multispectral imaging and LIBS. *arXiv*. https://arxiv.org/abs/2107.02355.
11. Iqbal, F., Lucieer, A., & Barry, K. (2018). *Simplified radiometric calibration for UAS-mounted multispectral sensor. European Journal of Remote Sensing*, 51(1), pp. 301–313. https://doi.org/10.1080/22797254.2018.1432293.
12. Keshet, D., Brook, A., Malkinson, D., Izhaki, I., & Charter, M. (2022). *The use of drones to determine rodent location and damage in agricultural crops*. Drones, 6(12), Article 396. https://doi.org/10.3390/drones6120396.
13. Korobeinikov, N. I., Peshkova, N. V., Valekzhanin, V. S., Boradulina, V. A., & Musalitin, G. M. (2014). *State Scientific Institution Altai Scientific Research Institute of Agriculture*.
14. Maimaitijiang, M., Ghulam, A., Sidike, P., Hartling, S., Maimaitiyiming, M., Peterson, K., Shavers, E., Fishman, J., Peterson, J., Kadam, S., Burken, J., & Fritschi, F. B. (2017). Unmanned aerial system (UAS)-based phenotyping of soybean using multi-sensor data fusion and extreme learning machine. *ISPRS*

*Journal of Photogrammetry and Remote Sensing*, 134, p. 43–58. https://doi.org/10.1016/j.isprsjprs.2017.10.011.

15. Mamaghani, B., Saunders, M. G., & Salvaggio, C. (2019). Inherent Reflectance Variability of Vegetation. Agriculture 2019, 9(11), p. 246; https://doi.org/10.3390/.
16. Masiri Kaamin, M. I. A., Faisal, M. H. A., Zaini, N. Z., Sahat, S., Mat Nor, A. H., Mokhtar, M., ... & Kamal, M. A. M. (n.d.). Production and evaluation of orthophoto map using UAV photogrammetry. Vol. 33 No. 1: December (2023). https://doi.org/10.37934/araset.33.1.187196.
17. Mazzia, V., Khaliq, A., Salvetti, F., Chiaberge, M., & Blotto, D. (2020). Improvement in crop monitoring through a deep learning framework for time series prediction. *Sensors*, 20(9), 2530. https://doi.org/10.3390/s20092530.
18. Mishra, A., & Singh, R. (2019). Chlorophyll monitoring with UAV imagery. *Precision Agriculture, 20*, pp. 65–80. https://doi.org/10.1007/s11119-018-09656-3.
19. Li, Y., Zhang, X., & Wang, J. (2020). Vegetation index applications in precision agriculture: A review. Agricultural Systems, 180, 102780. https://doi.org/10.1016/j.agsy.2020.102780.
20. Panthakkan, A., Murugan, A., & Ghosh, R. (2025). Evaluation of UAV-based RGB and multispectral vegetation indices for precision agriculture: A case study on palm trees. *arXiv*. https://arxiv.org/abs/2505.07840.
21. Peñuelas, J., Baret, F., & Filella, I. (1993). The soil-adjusted vegetation index (SAVI). International Journal of Remote Sensing, 14(8), pp. 1735–1745. https://doi.org/10.1080/01431169308954055.
22. Pu, R., Gong, P., & Yu, Q. (2008). Comparative analysis of EO-1 ALI and Hyperion, and Landsat ETM+ data for mapping forest crown closure and leaf area index. *Sensors*, 8(6), pp. 3744–3766. https://doi.org/10.3390/s8063744.
23. Rondeaux, G., Steven, M., & Baret, F. (1996). Optimization of soil-adjusted vegetation indices. *Remote Sensing of Environment, 55*(2), pp. 95–107. https://doi.org/10.1016/0034-4257(95)00186-7.
24. Serrano, L., Filella, I., & Peñuelas, J. (2000). Remote sensing of biomass and yield of winter wheat under different nitrogen supplies: Green normalized difference vegetation index (GNDVI). *Crop Science, 40*(3), pp. 723–731. https://doi.org/10.2135/cropsci2000.403723x.
25. Sullivan, J. (2006). Evolution or revolution? The rise of UAVs. *IEEE Technology and Society Magazine*, 25(3), pp. 43–49. https://doi.org/10.1109/mtas.2006.1700021.
26. Taddia, Y., Russo, P., Lovo, S., & Pellegrinelli, A. (2019). Multispectral UAV monitoring of submerged seaweed in shallow water. *Applied Geomatics*, 12(1), pp. 19–34. https://doi.org/10.1007/s12518-019-00270-x.
27. Wang, C. (2021). At-sensor radiometric correction of a multispectral camera (RedEdge) for sUAS vegetation mapping. *Sensors*, 21(22), p. 8224. https://doi.org/10.3390/s21248224.
28. Wang, F.-M., Huang, J.-F., Tang, Y.-L., & Wang, X.-Z. (2007). New vegetation index and its application in estimating leaf area index of rice. https://doi.org/10.1016/S1672-6308(07)60027-4.
29. Zhang, L., & Wang, S. (2007). Application of the WOFOST model in estimating wheat yield at the production level in northern China using MODIS data. *Journal of Zhejiang University-SCIENCE A*, *8*(5), pp. 834–841. https://doi.org/10.1016/S1672-6308(07)60027-4.
30. Zhang, X., & Wang, L. (2021). Monitoring wheat growth using UAV-based multispectral imagery. *Remote*

Vol. 64 No 02(254) 2025
DOI - https://doi.org/10.5564/pmas.v65i02.4390

*Sensing, 13*(12), p. 2345. https://doi.org/10.3390/rs13122345.

31. Zhu, W., Feng, Z., Dai, S., Zhang, P., & Wei, X. (2022). Using UAV multispectral remote sensing with appropriate spatial resolution and machine learning to monitor wheat scab. https://doi.org/10.3390/agriculture12111785.
32. Zhu, W., Rezaei, E. E., & Nouri, H. (2023). UAV flight height impacts on wheat biomass estimation via machine and deep learning. *IEEE Journal of Selected Topics in Applied Earth Observations and Remote Sensing*. https://doi.org/10.1109/JSTARS.2023.3302571.